LAWRENCE
LIVERMORE
NATIONAL
LABORATORY

LLNL-PROC-680378

The DSD Characterization of LX-17 with CHEETAH / ARES Front Data

J. Yao, L. Fried, P. Vitello

December 28, 2015

NEDPC 2015
Los Alamos, NM, United States
October 19, 2015 through October 23, 2015

Disclaimer

This document was prepared as an account of work sponsored by an agency of the United States government. Neither the United States government nor Lawrence Livermore National Security, LLC, nor any of their employees makes any warranty, expressed or implied, or assumes any legal liability or responsibility for the accuracy, completeness, or usefulness of any information, apparatus, product, or process disclosed, or represents that its use would not infringe privately owned rights. Reference herein to any specific commercial product, process, or service by trade name, trademark, manufacturer, or otherwise does not necessarily constitute or imply its endorsement, recommendation, or favoring by the United States government or Lawrence Livermore National Security, LLC. The views and opinions of authors expressed herein do not necessarily state or reflect those of the United States government or Lawrence Livermore National Security, LLC, and shall not be used for advertising or product endorsement purposes.

The DSD Characterization of LX-17 with CHEETAH / ARES Front Data

Jin Yao, Laurence E. Fried, and Peter A. Vitello

Lawrence Livermore National Laboratory

7000 East Avenue, Livermore, CA 94551

ABSTRACT

To adequately predict the behavior of a hydrodyamic system involving condensed phase detonation phenomena requires fine local zoning to resolve the reaction zone. Current computing power is not sufficient to provide a solution of this problem for many conventional high explosives. Adaptive mesh refinement (AMR) is a possibility, but its implementation is usually not trivial. The detonation shock dynamics (DSD) derives a relationship between detonation front velocity, curvature, and acceleration, and can be used to predict the front in space-time efficiently, with a front tracking (or capturing) method. Several DSD codes have been implemented. However the characterization with DSD for HE materials needs to be adequately obtained for these DSD codes to be useful in practice.

The traditional way to parameterize DSD is through experimental front geometry data. For many materials this data is not available, but reactive burn direct numerical simulation (DNS) models have been established that match experimental detonation velocity size effect and other experimental data. A common description of DSD characterization includes a $D_n(\kappa)$ curve for a range of curvatures, and a boundary intersection angle. Generally the $D_n(\kappa)$ relation is a property for the HE material away from boundary, but the boundary angle is a property of both the explosive and the confinement. A DSD algorithm can be accurate for description of detonation fronts and costs little compared to spatially resolved DNS with a reactive flow model. Therefore the DSD characterization of HE materials (coupled with confinements) is valuable for numerical simulation of material interaction involving detonation phenomena.

We describe a mathematical approach to obtain the DSD characterization from bare rate-stick experiments or copper lined cylinder expansion tests.. With the result of our DSD calibration, and utilizing our particle based DSD tracker (called SDOT, which stands for surface-dynamical-operation-tool), we are able to closely reproduce the detonation fronts generated from DNS in cylinder tests and other detonation problems.

DSD models are not traditionally applied to converging geometries. We describe a physically motivated modeling framework for DSD in converging geometries, based on the approximate size scaling of a spherical implosion.

PROCEDURE OUTLINE:

We take LX-17 as an example explosive material for this study. For many HE materials experimental data for direct experimental calibration of DSD are insufficient and difficult to obtain. However, DNS data is relatively easy to obtain for many insensitive high explosives with established reactive burn models. In this case we desire only that the DSD model be able to match the performance of DNS.

We first obtain the data from direct simulations with CHEETAH / ARES and the LLNL HE Validation Suite for a given material and propose a format for the DSD evolution equation (a relation between detonation shock velocity, front curvature and acceleration). We integrate the proposed evolution equation to match the DNS results by adjusting parameters using an optimization method. We use an efficient DSD tracker to compute a numerical front and match the DNS result, thus confirming that our DSD calibration is useful in practice.

SOME ISSUES WITH DSD APPLICATION

The $D_n(\kappa)$ curve, its turning points at the critical curvatures

With the best of our knowledge, the DSD governing equations used in existing DSD codes are all of the format $D_n = D_n(\kappa)$, i.e. the detonation velocity D_n is a function of the detonation front curvature κ . In theory, for an explosive material with large activation energy, such a $D_n(\kappa)$ relation has turning points and the curvature is bounded between a pair of critical curvatures. In (fig. 1), the turning point on the bottom stands for a radius of curvature necessary for ignition; the right-most turning point is at the failure curvature; finally, the turning point in the region of negative curvature means that a detonation is impossible to be steady if the curvature is too big.

The $D_n(\kappa)$ curve described above does not take the acceleration of the detonation front with respect to time into account. We will show that such a DSD law is sometimes insufficient in practice.

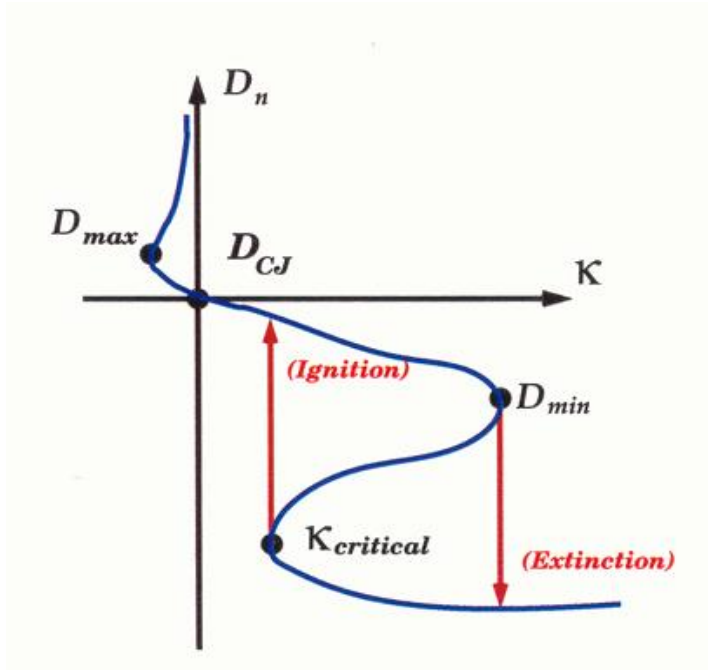

Figure 1. Demonstration of a $D_n(\kappa)$ curve that describe a quasi-steady detonation for an explosive of large activation energy. The effect of front-acceleration is ignored.

Acceleration vs. no acceleration

In a front-tracking simulation, there is no guarantee that a numerically generated detonation front has a curvature everywhere in the valid range at all time. A common practice is to manipulate a $D_n(\kappa)$ curvature and assign special values for velocity when the curvature is out of range. We believe this is not a natural treatment. We propose a DSD evolution equation for LX-17 with a relationship that involves not only the detonation velocity and curvature, but also the detonation acceleration. As a result, in the case the magnitude of curvature exceeds the valid range of a steady $D_n(\kappa)$ relation somewhere in the front, the acceleration effect would flatten the front, and there is no cut-off velocity values required. We consider our treatment to be more natural than the other one.

A converging detonation front

The DSD theory is derived under the assumption that a sonic point exists in the reaction zone, where the thermicity parameter and sonic parameter must both vanish. This condition sets a constraint to the evolution equation. This so called generalized CJ condition usually only holds for a diverging detonation, i.e. the front curvature is positive. The behavior of a converging detonation has not been well investigated. From the literature we see a common treatment in the case of negative curvature is to extrapolate a $D_n(\kappa)$ curve for positive curvature in to the region of negative curvature. Although the assumption of completion of reaction at the sonic point gives the conclusion of another turning point in the region of negative curvature, our direct numerical

simulation with CHEETAH has shown that such a single $D_n(\kappa)$ is not adequate for the case of a spherically converging detonation wave. However after the acceleration effect is employed, the front tracking with our calibrated DSD evolution equation produces results in agreement with DNS. Therefore we believe the acceleration term in a DSD evolution equation is necessary to describe the behavior of a detonation front with locally negative curvature.

The critical curvature and the failure velocity

With a rate-stick experiment, the front geometry and velocity can be observed (fig. 2). In principle because the data contains velocity and curvature information, a $D_n(\kappa)$ curvature can be obtained directly from experimental data. However, a set of rate-stick data covers only a small range of curvature for a limited set of experimental conditions. The current rate-stick data base for LX-17 is not sufficient to obtain a $D_n(\kappa)$ curve for a sufficiently large range of curvatures (or temperature, density…). Especially, the measurement of data close to boundary (where curvature is relatively large) is difficult to obtain. As a result, we lack experimental $D_n(\kappa)$ data in the region of large front curvature, thus the right-most turning point on the $D_n(\kappa)$ can not be obtained from rate-stick experiments (for LX-17 in this case, see fig. 2). However we may argue that in a corner-turning experiment, at the contact point when a detonation front just starts to turn the corner, the curvature is theoretically positive infinity. The trace of the high curvature 'cusp' defines the boundary of a dead-zone. This point must move with the failure velocity in the front normal direction because of continuity of velocity. Numerical simulation with our particle based DSD tracking package SDOT has shown the size and shape of a dead-zone in a corner-turning experiment with PBX-9502 can be obtained reasonably well by employing a proper $D_n(\kappa)$ law and failure velocity. The geometry of a numerically produced dead-zone seems not depend on the exact value of a critical curvature (because the time takes to exceed any preset critical curvature is very much *ignorable*). The geometry of dead-zone is in fact very insensitive to the input value of the critical curvature. We conclude that a proper failure velocity, not a critical curvature, together with a $D_n(\kappa)$, defines the boundary of a dead-zone in our front tracking calculation. The failure velocity can be determined from the size effect with rate-stick experiments reasonably well. For LX-17, we choose to set the value of its failure velocity to 0.72 ($cm/\mu s$) based on data from the LLNL HE Reference Guide [1].

We conclude that the actual value of critical curvature is not important in a corner-turning dead-zone simulation with DSD wave tracking.

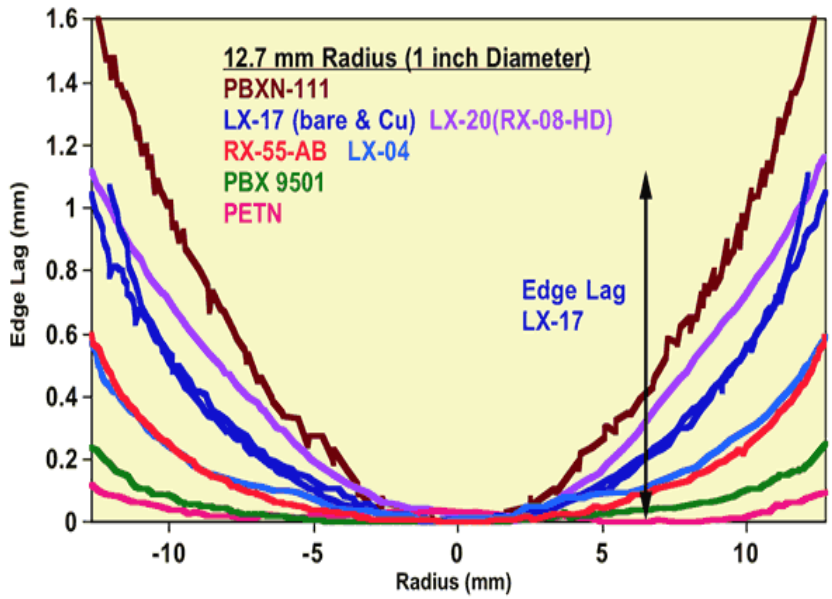

Figure 2. The experimental front geometries for a 12.7 mm radius rate-stick, including data of LX-17.

The Rate-Stick: A study of a steady diverging detonation

An HE rate-stick burn (bare or confined) is the most studied experiment. It has a steady state, independent of the initial detonation front geometry, with a constant traveling speed. Our DNS of rate stick is performed with CHEETAH / ARES. An effective DSD front-tracker should be able to reproduce the front geometry given a proper DSD front evolution equation in the format $D_n = D_n(\kappa, \dot{D}_n)$. For the purpose of this study we ignore the acceleration term $\dot{D}_n$ and calibrate a relation between the detonation front velocity and curvature that fits DNS data.

The geometry of a rate-stick is axisymmetric and is defined by the radius of the rate-stick. We set the axis of symmetry at $r = 0$ where r is the radius. The detonation front is moving up and forms a preset angle ω at the boundary, which is a property of the coupling of the HE and the confinement (fig. 3).

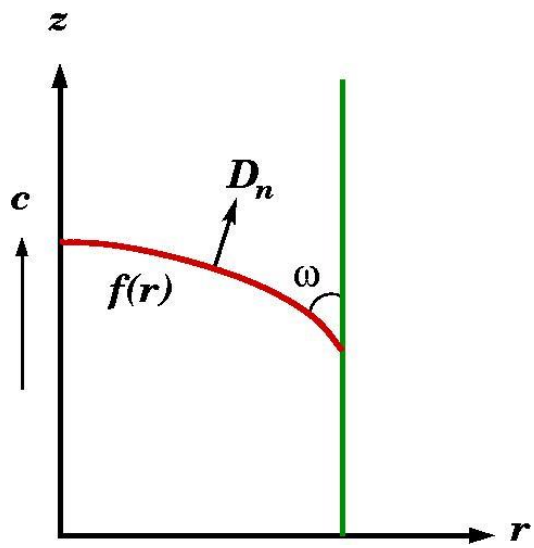

Fig.3. The rate stick geometry: $f(r)$ is the steady-state detonation front; c is the steady-state velocity; D_n is normal velocity; ω is the boundary intersection angle. $D_n = c/\sqrt{(1+f_r^2)}$.

A least-squared local fitting to obtain an initial guess of $D_n(\kappa)$

We take the detonation front geometry from the CHEETAH/ARES simulation of a cylinder-test for LX-17 with Cu confinement. The DNS data contains the steady state velocity U, the rate-stick radius R, and the shock arrival times at a set of points distributed on the radius at a selected position. The front geometry is conveniently computed as the product of the shock arrival time and the steady state front velocity. Using a least-squared quadratic local smoothing method, one is able to compute the front slope and curvature data pairs for the region away from boundary.

We pick a search length $\boldsymbol{s}$ much smaller than the rate-stick radius $\boldsymbol{R}$, but greater than the distance between data points. At a given $\boldsymbol{r}$, we fit a least-squared quadratic curve for the curvature and slope. From the front slope and the steady travelling speed, the normal detonation velocity is obtained. By varying $\boldsymbol{r}$ from *0* to $\boldsymbol{R}$, we obtain a set of (D, κ) data pairs. The data points are coarse and we take *10* points or so to perform each local fitting. At a point near the boundary, since there is no data outside of the boundary, the quality of fitting is not reliable. Therefore we choose to discard fitting results close to the boundary. Near the symmetrical axis a reflection of the data provides support to the least-squared fitting. Because the steady-state front velocity is provided with the DNS, we can convert slope to normal front velocity directly and obtain D_n (κ) pairs for a range of curvature by varying the point at which the fitting is performed.

The exact shape of $D_n(\kappa)$ in the region of high curvature is difficult to determine. However, we have discussed previously that only the failure velocity is important (at least in the case of corner-turning) because the time-space window for high curvature to live is so tiny that the exact value of curvature at the failure point takes almost no effect in a front-tracking simulation.

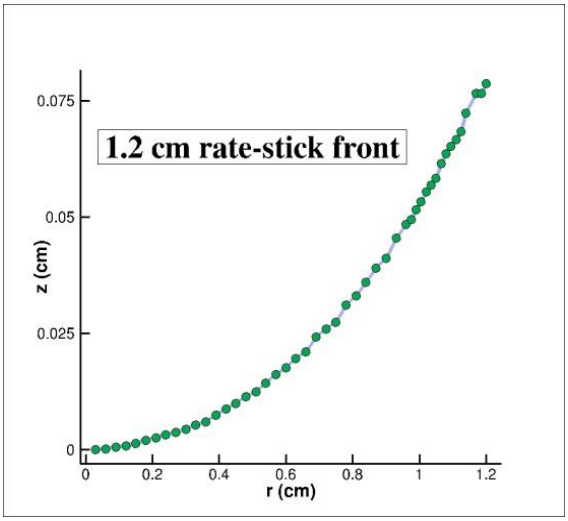

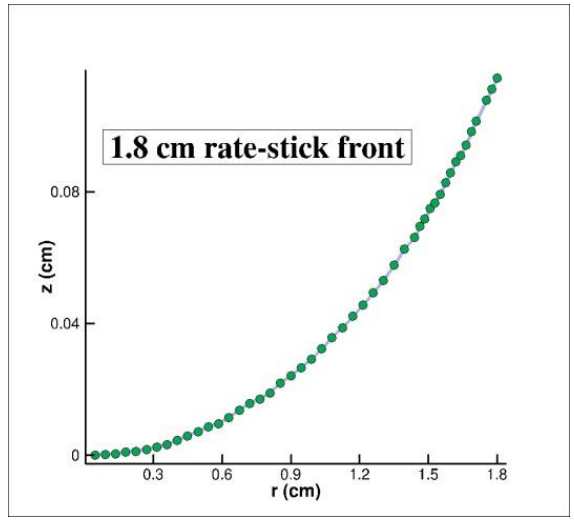

4(a). Front speed = 0.7556 (cm / μs). *4(b). Front speed = 0.7593 (cm / μs).*

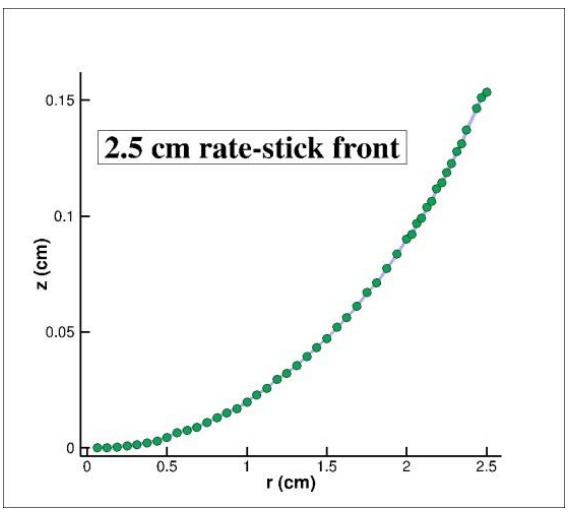

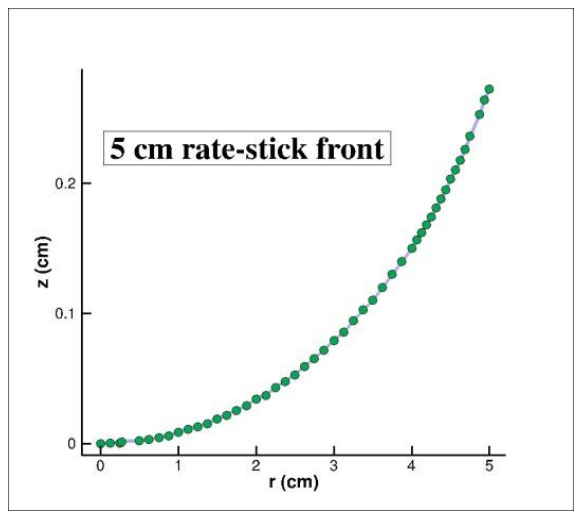

4(c). Front speed = 0.7629 (cm / μs). *4(d). Front speed = 0.7673 (cm / μs).*

Figure 4. The rate-stick steady front geometries obtained from DNS with CHEETAH / ARES for various radii: (a) r = 1.2 cm; (b) r = 1.8 cm; (c). r = 2.5 cm; (d) r = 5.0 cm.

The CJ velocity, the size effect, and the failure velocity of LX-17

To construct a $D_n(\kappa)$ formula for LX-17, some mandatory constraints need to be satisfied. For example, at the point of zero-curvature, one must have D_n equal to the CJ velocity. It is

impossible to observe the CJ velocity because a detonation front is never truly flat in a steady state experiment. The assumption is that D_{CJ} = 0.7734 (cm / μs) [13], based on extrapolation of the detonation velocity to infinite diameter. For the CHEETAH model, the infinite diameter detonation velocity has been calibrated to this value. However, the exact value of D_{CJ} used does affect our optimization scheme for calibration of DSD parameters here.

The failure velocity of LX-17 can be checked out from tables in the LLNL. It is observed at about 0.72 (cm / μs) with small variations depending on experimental conditions. With a rate-stick test, the smaller is the radius, the slower is the front velocity. Our DNS simulations with very slender rate sticks do not show a smooth drop of front velocity, probably because of an existing resolution issue. In our calibration, data for thicker rate-sticks are employed.

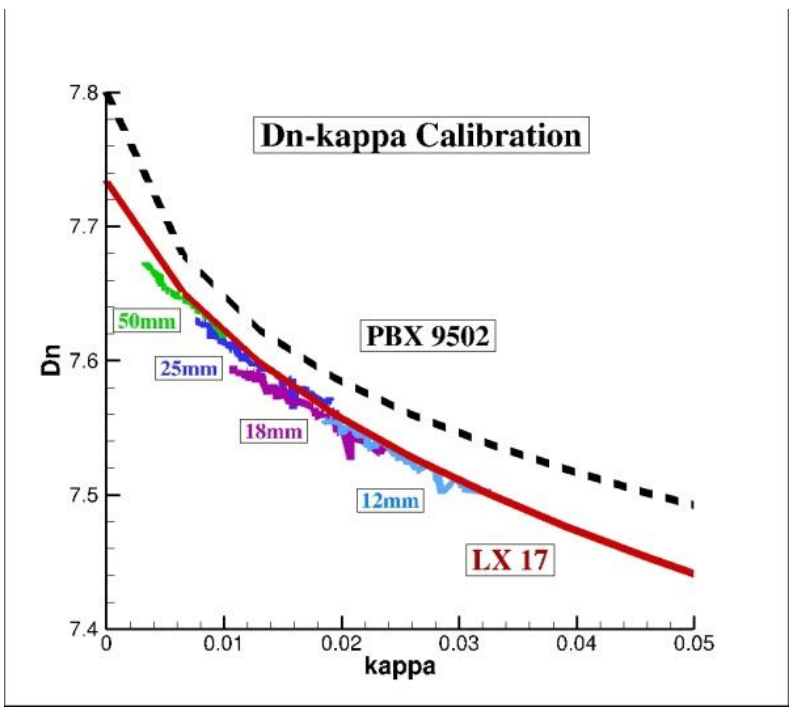

Figure 5. The $D_n(\kappa)$ data obtained form local least-squared fitting of rate-stick front geometries. Four sets of data are used for rate-stick radius of 50(mm), 25(mm), 18(mm) and 12(mm). The steady $D_n(\kappa)$ for PBX-9502 by Aslam, Hill and Bdzil [9] is also plotted for reference.

The rate-stick ODE

With the rate-stick geometry, one is able to convert the partial differential front governing equation into an ordinary differential equation of first order with the front slope as the independent variable. Numerical integration of the ODE over the range of radius using a given

mathematical $D_n(\kappa)$ relation provides geometry of a numerical front, by minimizing the difference between this numerical front and the given DNS data, one is able to determine the parameters in the mathematical $D_n(\kappa)$form for a calibrated solution of the detonation velocity-curvature relation for a given HE material, LX-17 in this case.

The DSD governing equation is a PDE in the form $\frac{\partial \phi}{\partial t} + D_n|\nabla\phi| = 0$.

For convenience we assume a mathematical form of the velocity-curvature relation that

$$\kappa = K(D_n). \tag{1}$$

We may take $\phi = z - f(r,t)$, then in the r-z coordinate the above PDE can be written as:

$$f_t - D_n(\kappa)\ (1 + f_r^2)^{\frac{1}{2}}. \tag{2}$$

Here the function $\phi = 0$ is the front position at time t and radius r. When the steady state is achieved, one has $f = ct + g(r)$ where c is the steady state propagation velocity, then the above equation becomes

$$c = D_n\ (\kappa)(1 + f_r^2)^{1/2}. \tag{3}$$

This is an obvious geometrical relation because f_r is the front slope.

In the axisymmetrical geometry the front-curvature can be written as the following:

$$\kappa = \frac{f_{rr}}{(1+f_r^2)^{\frac{3}{2}}} + \frac{f_r}{r(1+f_r^2)^{\frac{1}{2}}} \tag{4}$$

Then by substituting eq. (3) into it, the $D_n(\kappa)$ relation (1) becomes eq. (5)

$$\frac{f_{rr}}{(1+f_r^2)^{\frac{3}{2}}} + \frac{f_r}{r(1+f_r^2)^{\frac{1}{2}}} = \mathrm{K}[\frac{\mathrm{c}}{(1+f_r^2)^{\frac{1}{2}}}] \tag{5}$$

By setting $s = f_r$ being the slope of the front and the above equation becomes

$$\frac{s_r}{(1+s^2)^{\frac{3}{2}}} + \frac{s}{r(1+s^2)^{\frac{1}{2}}} = \mathrm{K}[\frac{\mathrm{c}}{(1+s^2)^{\frac{1}{2}}}]$$

or equivalently

$$s_r = \left(\mathrm{K}\left[\frac{\mathrm{c}}{(1+s^2)^{\frac{1}{2}}}\right] - \frac{s}{r(1+s^2)^{\frac{1}{2}}}\right)(1 + s^2)^{\frac{3}{2}}. \tag{6}$$

Thus the above equation is an ODE that governs the front geometry of the steady-state in a rate-stick problem (and we call it the *rate-stick ODE*). In the case of planar 2D geometry, the term *s/r* is dropped out and an explicit first integral can be evaluated for certain choices (say linear) of the function *K*.

The choice of the mathematical form of the $D_n(\kappa)$ curve for LX-17 is not arbitrary but is not unique. We have performed an optimization for linear form of $D_n(\kappa)$ curve and it works rather well for individual tests. However we consider a global $D_n(\kappa)$ curve that has a turning point at the failure velocity and propose the following form for the $D_n(\kappa)$ relation for LX-17.

$$\kappa = \alpha(e^{\beta g(D_n)} - 1), \text{ where } g(D_n) = (D_n - D_{fail})^{\gamma} - (D_{CJ} - D_{fail})^{\gamma}. \quad (7)$$

With D_{CJ} is set to 0.7734 (*cm/μs*) and D_{fail} set to 0.72 (cm/μs), α, β, and γ are free parameters. This curve has a bell shape and a turning point exists at $D_n = D_{fail}$.

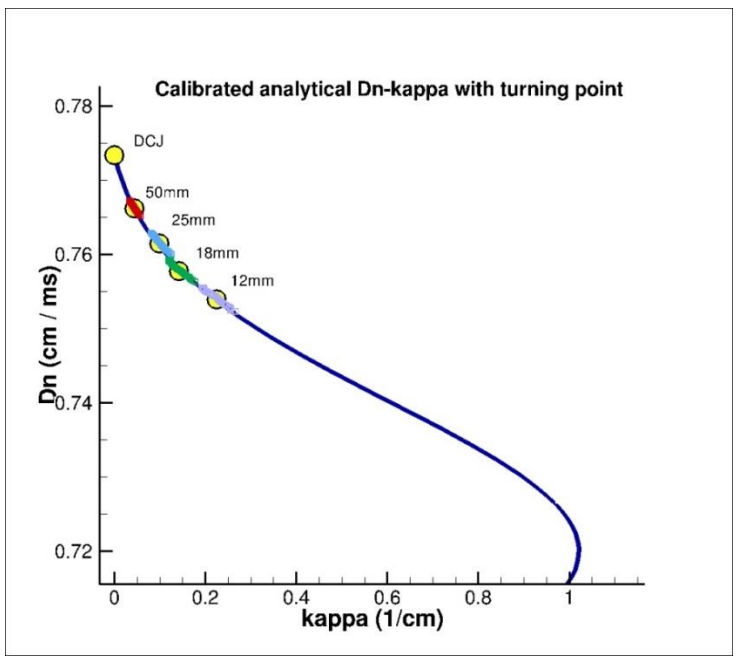

Figure 6. The proposed bell-shape $D_n(\kappa)$curve with a turning point at D_{fail} for LX-17. Only the portion of positive curvature (i.e. for a diverging detonation) is shown in the figure.

Optimization for DSD characterization of LX-17

The slope $s = f_r$ of a rate-stick detonation front at any given *r* can be computed with a numerical integration of eq. (6). Then the front geometry can also be determined by integration in the r-direction. If the $D_n(\kappa)$ curve is correctly given, the integrated front geometry should match the input front geometry. By minimizing the difference between the two front geometries, the coefficients that determine the $D_n(\kappa)$ curve can be determined.

Now we start our calibration for DSD characterization of LX-17. The target function for minimization is defined as

$$J(\alpha,\beta,\gamma) = \frac{1}{2}\sum\left(f_i^{integrated} - f_i^{input}\right)^2. \qquad (8)$$

Where $f_i^{integrated}$ stands for position of the front from numerical integration of the rate-stick ODE at data point 'i', f_i^{input} is the input data shown in fig. 4 at the same point. We use a Runge-Kutta 4th order scheme to integrate the rate-stick ODE. All the input data point gets an equal weight and all the four sets of rate-stick data are used.

Because of the highly nonlinear format of (eq. 7), a bad initial guess constantly results in non-convergence. We used a carpet search to obtain a set of reasonable initial guess $(\alpha_0, \beta_0, \gamma_0)$ for the $D_n(\kappa)$ coefficients. For simplicity we first tried not to compute multi-dimensional derivatives of the function *K*, but to walk in one-dimension at a time and alternating directions (the coordinate-descent method).

Starting from *k = 0*, at step *k* we perform the following operations:

In the alpha-direction:

Fixing β_k, γ_k, compute three values $J(\alpha_k + d\alpha, \beta_k, \gamma_k)$,$J(\alpha_k, \beta_k, \gamma_k)$,$J(\alpha_k - d\alpha, \beta_k, \gamma_k)$, then fit a quadratic $P = A + B\alpha + Ca^2$. Then find the minimization point $\alpha_{k+1} = -B/2C$. This is a third order approximation in the α-direction.

In the beta-direction:

Fixing α_{k+1}, γ_k, compute three target values $J(\alpha_{k+1}, \beta_k + d\beta, \gamma_k)$,$J(\alpha_{k+1}, \beta_k, \gamma_k)$,$J(\alpha_{k+1}, \beta_k - d\beta,\ \gamma_k)$, then fit a quadratic $Q = D + E\beta + F\beta^2$. Then find the minimization point $\beta_{k+1} = -E/2F$. This is a third order approximation in the β-direction.

In the gamma direction:

Fixing $\alpha_{k+1}, \beta_{k+1}$, compute three values $J(\alpha_{k+1}, \beta_{k+1}, \gamma_k + d\gamma)$,$J(\alpha_{k+1}, \beta_k, \gamma_k)$,$J(\alpha_{k+1}, \beta_{k+1}, \gamma_k - d\gamma)$, then fit a quadratic $R = G + H\gamma + I\gamma^2$. Then find the minimization point $\gamma_{k+1} = -H/2I$. This is a third order approximation in the γ-direction.

Let *k* be increased by *1*, repeating the above operations till convergence. In the region of curvature in a given rate-stick problem, there is no turning point on the $D_n(\kappa)$ curve, thus three control parameters (α, β, γ) are likely sufficient for a good DSD characterization in a relatively small region. These control parameters are equivalent to a set of control points with the number of points equal to the number of control parameters. With more data from rate-stick tests, it is possible to locate more control points for higher curvature region. These control points shall define the $D_n(\kappa)$ curve for a wider range of curvatures. The boundary intersecting angle, which

is assume a constant for a pair of HE/confinement coupling. If this is true, we should be able to obtain similar values of s_w with rate-stick tests of different diameters for a certain HE/confinement coupling.

The calibrated solution with the above optimization scheme is obtained as the following $\boldsymbol{\alpha}$=$\mathbf{0.029842}$ $(\mathbf{1}/\boldsymbol{cm})$, β =$\mathbf{1246.1}(\boldsymbol{\mu s}/\boldsymbol{cm})^{\mathbf{2}}$, $\boldsymbol{\gamma}$=$\mathbf{2}$, D_{fail}=$\mathbf{0.719963}$ $(\boldsymbol{cm}/\boldsymbol{\mu s})$ for LX-17.

Numerical fronts obtained with rate-stick ODE integration compared to input DNS data

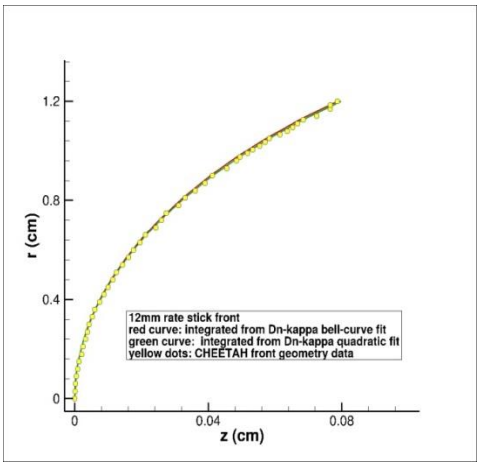

Figure (7a). the 12 (mm) rate-stick.

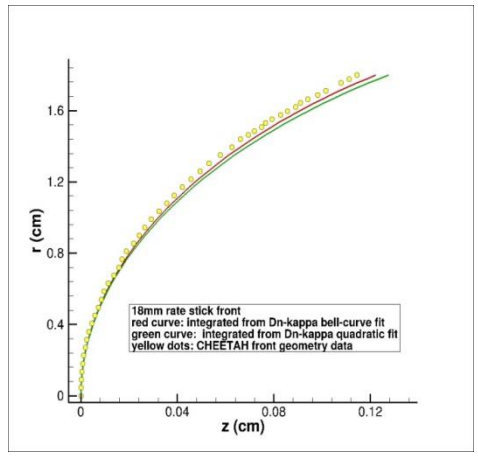

Figure (7b). the 18 (mm) rate-stick.

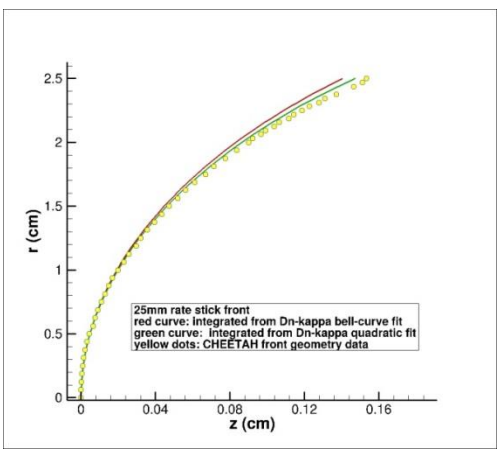

Figure (7c). the 25 (mm) rate-stick.

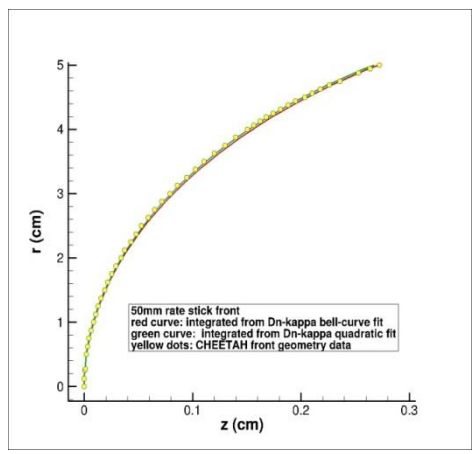

Figure (7a). the 50 (mm) rate-stick.

Spherical Imploding Detonation: A study of converging detonation waves

A $D_n(\kappa)$ relation has been shown to be able to predict the motion of a diverging detonation that has a positive curvature. A detonation can be converging in certain configurations. In this case, a quasi-steady detonation cannot be mathematically determined by the generalized CJ condition because the thermicity condition would not vanish with a positive detonation curvature. In the literature a common treatment is a simple extrapolation of the steady $D_n(\kappa)$ curve for a diverging

detonation into the region of positive curvature. Forcing the completion of a detonation occurs at the sonic locus indicates that a third turning point must exist in the region of negative curvature [12]. However there has been no experimental result to support this conclusion. The issue of using DSD to predict the motion of front with negative front curvature has not been well addressed. In this study we performed DNS simulations for a spherically converging detonation with various initial detonation sphere radii. The results show that a steady $D_n(\kappa)$ does not explain the size effect. However we observed approximately a unique solution that depends on the relative radius. Under the assumption that the motion of the wave front of a spherical converging detonation can be described by a surface evolution law, we propose a relation between curvature and acceleration in the case of an over-driven detonation.

The DNS result for a spherically converging LX-17 detonation

A series runs of one dimensionally spherically converging detonation of LX-17 was performed with ARES runs using the Ignition and Growth reactive burn model. The Ignition and Growth model was chosen since it is well-tested for a large variety of problems. A fine resolution of 64 zones/mm was chosen to ensure convergence of the results. The front-velocity is plotted against radius with the initial radii 10 mm, 20 mm, 40 mm, and 80 mm in fig. 8.

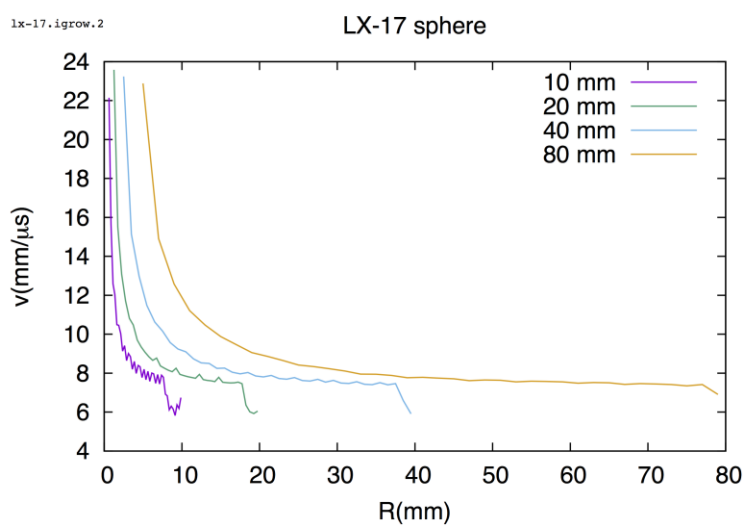

Figure 8. Front velocity vs. radius plot for DNS simulation of a spherically converging LX-17 detonation for initial radii of 10 mm, 20 mm, 40 mm, and 80 mm.

Because the front curvature is twice the inverse of the radius, the above plot is equivalent to a D_n (κ) plot. Since curves do not converge to a single one, this result means a converging spherical detonation cannot be described by a steady $D_n(\kappa)$ relation.

However, let the initial radius be R, we observed a unique curve that all solutions converge after shock initiation has finished in the space of the non-dimensional length variable r/R, shown in fig. 9.

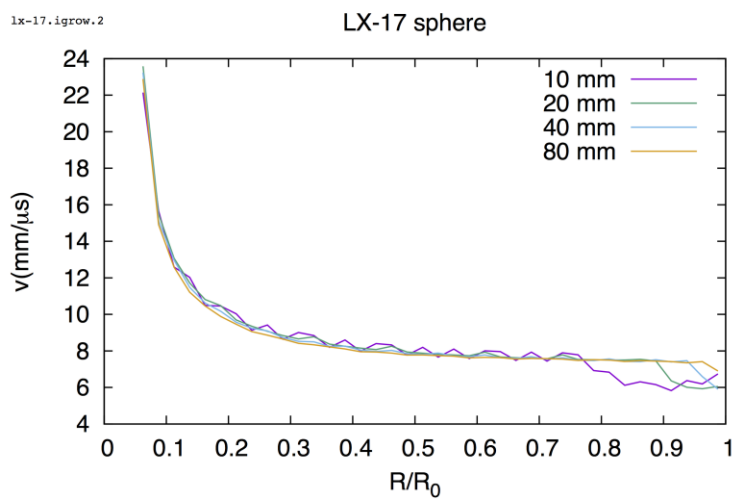

Figure 9. Front velocities vs. relative radius plot for the DNS simulation of a spherically converging LX-17 detonation. R is the position of the detonation front, and R_0 is the initial position of the detonation front. Except the part near initial radius where the detonation is being initialized, all the curves collapse to a single one.

A velocity-curvature-acceleration front evolution law for LX-17

To describe a spherically converging detonation, we propose a velocity-curvature-acceleration relationship as the follows

$$\dot{D_n} = -\frac{1}{2}\kappa D_n f(D_n). \qquad (9)$$

Where the curvature κ can be expressed with (*-2 / r*), the front velocity $D_n = -\frac{\partial r}{\partial t}$, the negative sign is for the detonation is moving inward. This relation has the dimensional scaling demonstrated in fig. 8: if the system size is doubled (thereby halving κ), the acceleration of D_n is halved. Applying the chain rule we have $\dot{D_n} = -\frac{dD_n}{dr} \times D_n$.

$f(D_n)$ is a material-dependent function. Therefore from the proposed mathematical form in (eq. 9), one arrives at

$$\frac{dD_n}{f(D_n)} = \frac{dr}{r}, \quad \text{or} \int \frac{dD_n}{f(D_n)} = \log(r). \qquad (10)$$

We have employed the form $f(D_n) = \frac{(D_n - a)^2}{c}$ for LX-17 and derived an explicit solution:

$$\frac{c}{D_n - a} - b = \log\left(\frac{r}{R}\right). \qquad (11)$$

R is the initial detonation radius. a, b, c are constants that can be determined with fitting of the shock arrival time. We define a least-squared target function for optimization that

$$T = \frac{1}{2}\Sigma_k \left(\frac{c}{D_n^{[k]} - a} - b - \log\left(\frac{r^{[k]}}{R}\right)\right)^2 , \qquad (12)$$

where k is an integer iterating through all the data sets from the DNS results. With a quasi-newton method using numerical derivatives, we obtain the solution of optimization that

$$a = 0.344906\left(\frac{cm}{\mu s}\right),\ b = 3.301576,\ c = 1.07931\left(\frac{cm}{\mu s}\right) \text{ for LX-17.}$$

The solution is plotted below

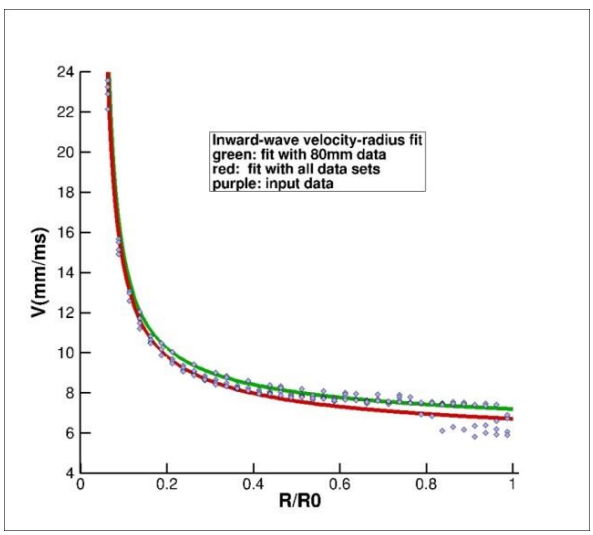

Figure 10. Input data vs. the solution with optimization for a spherically converging detonation. The red curve is lower than the green one because some of the data points are from initialization (the points with velocity below the CJ value (r/R > 0.8). DSD is effective after the initialization.

A combined velocity-curvature-acceleration model

We have calibrated a D_n (κ) for *positive curvature* that fits the rate-stick data from DNS.

$$\kappa = K(D_n) = \alpha\left(e^{\beta g(D_n)} - 1\right),$$

$$g(D_n) = \left(D_n - D_{fail}\right)^{\gamma} - \left(D_{CJ} - D_{fail}\right)^{\gamma} \qquad (13)$$

We have also calibrated a $\dot{D_n}(D_n, \kappa)$ for negative curvature with spherically converging wave data from DNS

$$\dot{D_n} = -\frac{1}{2}\kappa D_n f(D_n),$$
$$f(D_n) = \lambda(D_n - \mu)^2. \qquad (14)$$

We hope to combine them with a mathematical form that works in both the diverging and the converging cases. Our proposed formula is the follows

$$\dot{D_n} = -\frac{1}{2}(\kappa - K(D_n))D_n f(D_n). \qquad (15)$$

For the steady state in a rate-stick test, acceleration is small and the above formula is reduced to

$$\kappa = K(D_n) + \mathrm{h.o.t.} \qquad (16)$$

Then our previously obtained $D_n\ (\kappa)$ for a diverging detonation is recovered.

One can also verify that for an over-driven wave, an asymptotic line $K(D_n) = -\alpha$ is there, and α is a high order term ($h.o.t.$) compared to the magnitude of curvature ($2/r$) in the other case of the spherically converging tests as r goes to zero. Again, the formula is reduced to

$$\dot{D_n} = \frac{1}{2}\kappa D_n f(D_n) + \mathrm{h.o.t.} \qquad (17)$$

Therefore, our previously obtained $\dot{D_n}(D_n, \kappa)$ for a converging detonation is recovered. Our proposed formula reduces to the correct formula at both limits.

Fitting the DNS data with the combined velocity-curvature-acceleration relation

We have observed ignorable acceleration when the steady state front is formed in our SDOT simulations of rate-stick tests, therefore we do not bother to change the parameters in $K(D_n)$.

In the other case, since $K(D_n)$ becomes a small curvature correction plus an exponentially decaying term as D_n goes above D_{CJ} , we argue that the only complexity comes from the constant added to the curvature term. Luckily we again can explicitly integrate the combined velocity-curvature-acceleration equation. By fitting the input DNS data for a spherically converging LX-17 detonation once more, we obtained slightly different parameters with

$f(D_n) = \frac{(D_n - c)^2}{a}$, where a = 0.989 is a scalar, c = 0.403624 (cm / μs), which is very close to the sound speed of LX-17. The new fitting is plotted below

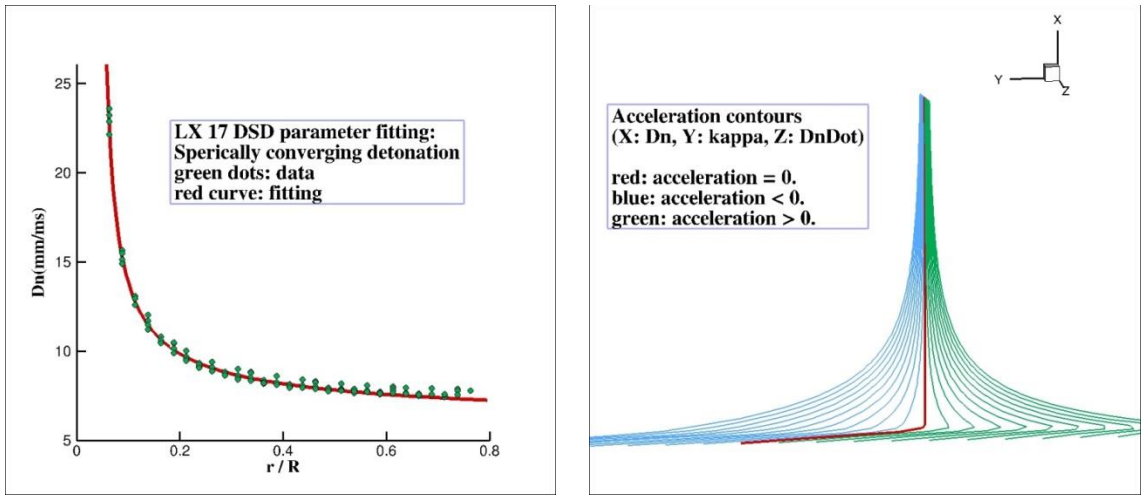

Figure 11. Figure on left: detonation velocity vs. radius. Red curve is a fit with the combined velocity-curvature-acceleration relation, the greed dots are DNS data. The right figure shows the acceleration contours of the calibrated $\dot{D}_n(D_n, \kappa)$ *, red curve is the steady* $D_n(\kappa)$ *(* $\dot{D}_n = 0$*).*

Introduction of the package SDOT (surface-dynamical-operation-tool)

SDOT (Surface Dynamical Operation Tool) is a compact numerical package that contains a particle DSD tracker, in development at LLNL. The following table roughly explains the meaning of the name of this package.

Character(s)	**Stands for**	**Meaning**
S	**First character of surface**	**Surface**
DOT	**Time rate (d/dt)**	**Dynamical evolution**
DOT	**Points (or particles)**	**Point (particle) based algorithms**
SDOT	$\dot{S}$ **(time rate of surface)**	**Surface dynamical Evolution**
SDOT	$\dot{S}$ **= ds/dt => DSDT**	**Detonation Shock Dynamical Tracker**
SDOT	**Initial characters for**	**Surface Dynamical Operation Tool**

SDOT performs the following numerical operation with high accuracy / efficiency and low cost: geometrical intersection/inclusion; front tracking that takes arbitrary boundary; HE modelling, interface reconstruction; and mesh relaxation / smoothing.

With a D_n (κ) function obtained from optimization and a boundary angle from the input data, the DSD tracker in SDOT is able to accurately recover the rate-stick front geometry.

The marked particle DSD tracker in SDOT

A detonation front is expressed by marked particles with this tracker. The motion of the particles is governed by a set of ODEs converted from the original partial differential DSD evolution equation [12] and can be integrated with 3rd order spatial accuracy. The positions of the moving particles at a given time define the numerical detonation front. Because at any given time, only the particle positions and boundary geometry need to be carried, the information needs to be dealt with at a time step is small. The tracker is accurate, compact, efficient, flexible front tracker.

Some of other features of SDOT tracking include the following. It uses control points and a geometry rule to express the HE boundary, thus it takes an arbitrary boundary and the boundary information is small (see figures. 8a, 8b). It also keep sharpness of profile (because intersection is used to deal with front intersection, see fig. 8b) when detonation fronts impact. It admits arbitrary initial front geometries as well. In addition, this particle tracker has the unique capability to simulate dead-zones in corner-turning tests.

The spatial complexity of a DSD tracking problem is down by a dimension. A whole problem is reduced to moving the particles on a detonation front at a given time. The SDOT DSD tracking is efficient. It also takes very small memory space compared to other DSD implementations. Parallization may not be necessary in 2D for even a rather large problem. If necessary, a parallelization can be performed with ease because the algorithm depends on locality.

Numerical examples with the SDOT DSD tracking

Some of SDOT DSD tracking front plots (time-contours) are shown on next page (figure 12a, 12b). The first one has a curved star-fish boundary geometry that is expressed by only 10 control points. The second one has a planar zig-zag boundary defined by only 12 points. Compared to a HE boundary with a PDE solving algorithm that requires many cell faces, even interface reconstruction to represent material boundaries, SDOT carries only the minimum required boundary information and can easily admit an arbitrary boundary geometry. This is clearly an advantage with SDOT. A major reason is that the SDOT boundary data can be shared by all processors in the case that parallelization is needed. The SDOT tracking is also uniquely capable of simulating a dead-zone in a corner-turning test. It turns out that a dead-zone is a geometrical necessity with forcing an acute DSD angle, under the assumption that a failure curvature exists with a certain failure speed of a given explosive material of large activation-energy.

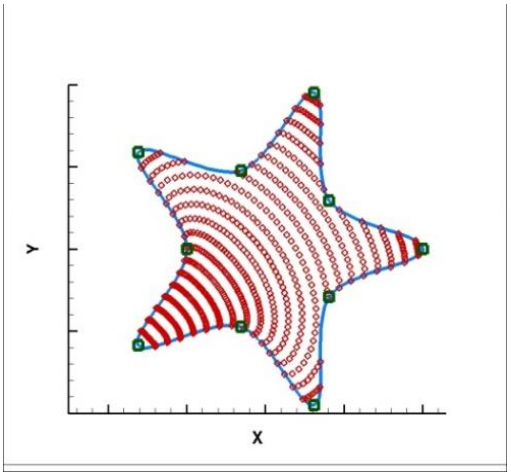

Figure 12a. This boundary is defined by 10 points and the rule of a cubic spline. A detonation point source is at the left foot.

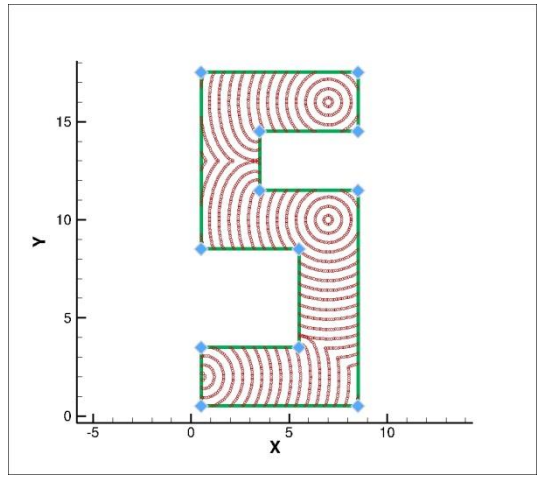

Figure 12b. This boundary is defined with 12 points and planar boundary faces. There are three detonation point sources.

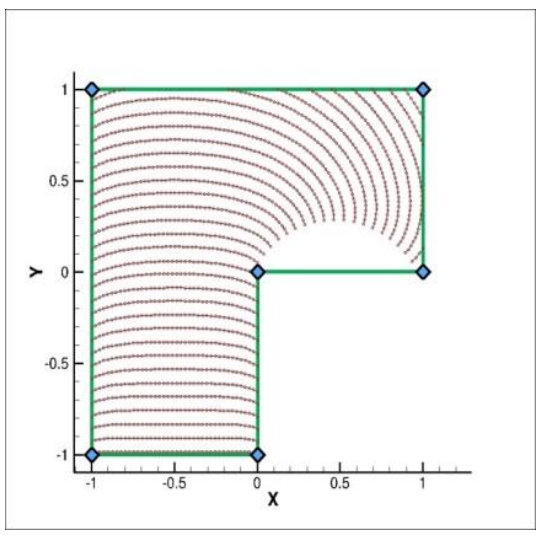

Figure 13 is a demonstration of dead-zone simulation with a simple corner-turning test. A linear $D_n\ (\kappa)$ is used to governing the motion of the initially flat front. The boundary intersection angle is set to $(\pi/3)$.

Simulation of dead-zones in a corner turning

The DSD theory predicts that when the detonation front curvature exceeds a critical value, the detonation speed arrives at a failure value and the corresponding detonation will not propagate. In a corner-turning test, a high curvature cusp appears at the corner and a dead zone is defined by the trace of the cusp. The cusp moves in the normal direction with the failure velocity for continuity of the speed. Tracing this cusp after the front has just passed the corner; a clear dead-zone structure appears (fig. 9). The mathematical reason for the cusp to touch down the boundary

again is that it moves slower than the particles away from it in the same front. Then the front normal naturally makes turn toward the boundary.

Comparison with LANL corner-turning experiments and DNS

We take a reasonable $D_n\ (\kappa)$ for PBX-9502 [8] and applied the SDOT DSD tracker. The simulated dead-zone structure is found to be in agreement to the LANL impact chamber experiment and direct numerical simulations [10]. We set the boundary intersection angle between front and the boundary to (π / 3). We also picked a failure velocity with which the time contours in [10] are roughly matched. It is possible to fine tune the DSD parameters to obtain a better match but it is not the focus in this paper. The dead zone boundary moves outwards once it is formed because of higher pressure in center pushed the dead-zone. There for at a later time, a snap shot of the dead zone will deform. This is consistent with the SDOT DSD tracking. In fig. 10, the density plot of the DNS result, the SDOT DSD tracking, and a series of snap shots of DNS at different times are shown. Since the purpose of our study is to obtain a DNS quality solution with a simple wave tracking, this result is encouraging.

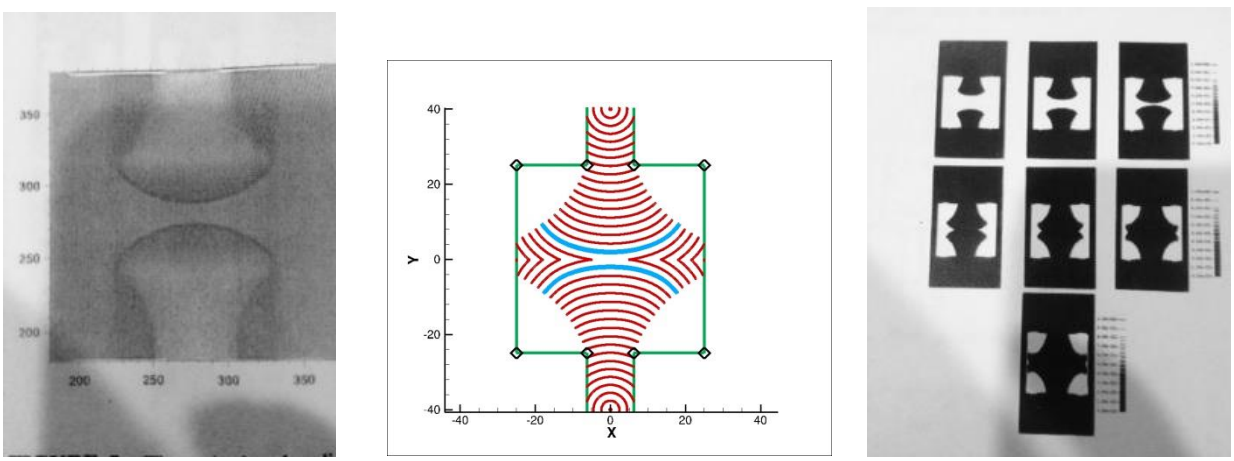

Figure 14. From left to right: DNS density plot at a single time; the SDOT time contours; the snap shot of DNS result at different times, all for the experimental set up in [10].

SDOT rate-stick tests with our combined velocity-curvature-acceleration model

With the $D_n\ (\kappa)$ function obtained from optimization and a boundary angle from the input data, our DSD tracker in SDOT accurately recovers the front geometry. Figure 15 shows the comparison of the front geometry by SDOT tracking with our calibrated D_n (κ) relation for LX-17 and by the DNS using CHEETAH / ARES.

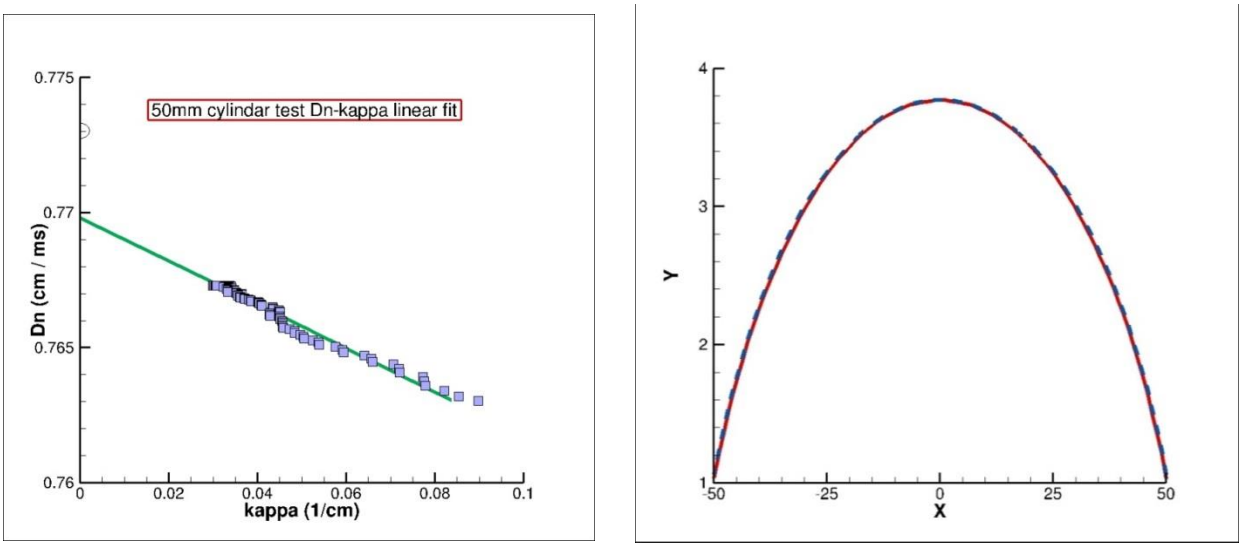

Figure 15 (a, b). A linear fit for the 50 (mm) rate-stick velocity-curvature pair, and comparison between front geometries by the SDOT tracking (dashed-blue curve) and DNS data (red curve).

Difference between numerical tracking using a DSD law with or without acceleration

With either the quasi-steady $D_n(\kappa)$ relation or the unsteady $\dot{D}_n(D_n,\kappa)$ relation calibrated for LX-17 previously, the steady state with a rate-stick test can be obtained with the SDOT DSD tracking method. We compared numerical results from applying the two different evolution laws with a zig-zag initial profile, and observed numerical differences.

First of all, the initial front is a zig-zag one that has high value of curvatures. With the steady $D_n\ (\kappa)$, one has to assign cut off values of the detonation velocity when curvature is out of the valid range. In the other hand, with the unsteady $\dot{D}_n(D_n,\kappa)$, a large curvature would be responded by a large acceleration against the increasing of curvature thus will quickly flatten high curvature. There is no need to assign any cut-off velocities in this case. Secondly, we observed that with the steady $D_n\ (\kappa)$, the front takes longer to reach the steady state than with the unsteady $\dot{D}_n(D_n,\kappa)$. Furthermore, their final states do not overlap in time (figure 16). This raises the question that which DSD evolution law is closer to reality. We have not yet performed DNS for comparison. However, we believe that the acceleration effect must exist in reality. Besides, the unsteady $\dot{D}_n(D_n,\kappa)$ does not need special treatment in the case that curvature is out of range, therefore is easier to implement. Furthermore we have shown that a converging detonation cannot be described with a steady $D_n(\kappa)$. Therefore we prefer the unsteady $\dot{D}_n(D_n,\kappa)$ over the steady $D_n\ (\kappa)$, because adding the acceleration makes more sense physically and is easier to deal with numerically. However, as far as we know, none of the existing DSD packages utilize a DSD front evolution law that includes acceleration, calibrated for a practical HE material. Since we are able to calibrate a velocity, curvature, acceleration

relation for LX-17 with this work, we would like to see the acceleration effect can be implemented in existing DSD packages with calibration of various explosives.

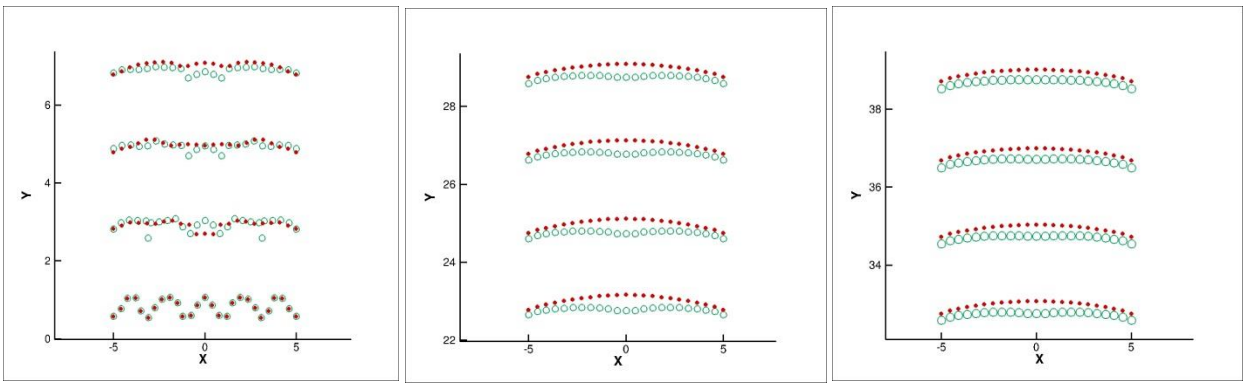

Figure 16 (a, b, c). The comparison between SDOT front-tracking solution of a 50 (mm) rate-stick test, with the steady $D_n(\kappa)$ (front expressed by green circles) and with the unsteady $\dot{D}_n(D_n, \kappa)$ (front expressed by red dots).

CONCLUSION

Accurate detonation front geometry can be predicted to the quality of DNS with an intrinsic velocity-curvature-acceleration relation. We have demonstrated this with LX-17 with a calibrated explicit formula, for both diverging and converging waves in certain cases. Our approach is purely numerical and can probably be applied to other HE materials.

Prepared by LLNL under Contract DE-AC52-07NA27344.

REFERENCES

[1]. P. Clark Souers, and others, The LLNL Explosives Reference Guide, *LLNL-WEB-667627*, 2015.

[2]. T. Aslam, J. Bdzil, and D. S. Stewart, “Level-Set Techniques Applied to Modeling Detonation Shock Dynamics”, *Journal of Computational Physics*, 126, 390-409, 1996.

[3]. J. B. Bdzil, R. J. Henninger, and J. W. Walter, “Test Problems for DSD2D”, *LA-14277*, 2006.

[4]. M.A. Kenamond, “HE Burn Table Verification Problem”, *LA-UR 11-03096*, 2011.

[5]. J. Yao, “A Geometrical DSD Lighting Algorithm on Arbitrary Unstructured Meshes”, *UCRL-JRNL-213932*, Lawrence Livermore National Laboratory, 2005.

[6]. J. Yao, "A Time Dependent ODE Conversion of the Detonation Shock Dynamics Evolution Equation", *LLNL-TR-641948*, August 6, 2013.

[7]. J.A. Sethian, “Level Set Methods and Fast Marching Methods”, Cambridge University Press, 1999.

[8]. Larry G. Hill and Tariq D. Aslam, “Detonation Shock Dynamics Calibration for PBX 9502 with Temperature, Density, and Material Lot Variations”, *Fourteenth International Detonation Symposium*, Coeur d'Alene Resort, Idaho, 2010.

[9]. T. D. Aslam, J. B. Bdzil and L. G. Hill, “Extensions to DSD Theory: Analysis of PBX 9502 Rate Stick Data”, *Eleventh International Detonation Symposium*, 1998.

[10]. Charles L. Mader, John D. Zumbro, and Eric N. Ferm, “Proton Radiographic and Numerical Modeling of Colliding, Diverging PBX-9502 Detonations”, *Thirteenth International Detonation Symposium*, 2002.

[11]. J. Yao, and Scott Stewart, “The Turning Points on a $D_n(\kappa)$ Curve”, *SIAM Conference on Numerical Combustion*, Monterey, CA, 2008.

[12]. J. Yao, “A Mesh-free DSD Front Tracker for an Arbitrary HE Boundary”, *Fifteenth International Detonation Symposium*, San Francisco, 2014.

[13]. Private communication with Larry Fried, Clark Souers, and Peter Vitello, *LLNL*, 2014.